Food Chemistry 378 (2022) 132061

Contents lists available at ScienceDirect

Food Chemistry

journal homepage: www.elsevier.com/locate/foodchem

A phage virus-based electrochemical biosensor for highly sensitive detection of ovomucoid

Jae Hwan Shin [a], Tae Jung Park [b], Moon Seop Hyun [c], Jong Pil Park [a,*]

[a] Basic Research Laboratory, Department of Food Science and Technology, Chung-Ang University, Anseong 17546, Republic of Korea
[b] Department of Chemistry, Institute of Interdisciplinary Convergence Research, Research Institute of Chem-Bio Diagnostic Technology, Chung-Ang University, 84 Heukseok-ro, Dongjak-gu, Seoul 06974, Republic of Korea
[c] National NanoFab Center (NNFC), 291 Daehangno, Daejeon 34141, Republic of Korea

ARTICLE INFO

Keywords:
M13 phage
Chemical modification
Ovomucoid
Electrochemical phage sensor

ABSTRACT

Whole peptide-displayed phage particles are promising alternatives to antibodies in sensor development; however, greater control and functionalization of these particles are required. In this study, we aimed to identify and create highly sensitive and selective phage-based electrochemical biosensors for detecting ovomucoid, a known food allergen. Phage display was performed using two different phage libraries (cyclic and linear form of peptides), which displayed affinity peptides capable of binding specifically to ovomucoid. Throughout the biopanning, two phage clones that displayed both peptides (CTDKASSSC and WWQPYSSAPRWL) were selected. After the characterization of their binding affinities, both whole phage particles were covalently attached to a gold electrode using crosslinking chemistry (MUA-EDC/NHS and Sulfo-LC/SPDP); the developed phage sensor was characterized using cyclic voltammetry (CV), square wave voltammetry (SWV), and electrochemical impedance spectroscopy (EIS). The cyclic peptide-displayed phage sensor modified using EDC/NHS chemistry exhibited significantly better binding affinity ($K_d = 2.36 \pm 0.44$ μg/mL) and limit of detection (LOD, 0.12 μg/mL) for ovomucoid than the linear phage sensor, resulting in good reproducibility and recovery, even in an actual egg and white wine samples. This approach may provide an alternative and more efficient way of sensing food allergens with desirable sensitivity, selectivity, and feasibility in food diagnostic applications.

1. Introduction

Food allergy is emerging as an important public health problem in modern society (De Martinis et al., 2020). Among the various food allergies, eight have been found to be the most common food allergies worldwide (Galan-Malo et al., 2019). Egg allergy, one of the eight major allergies, frequently occurs in young children (Caubet & Wang, 2011), with incidence of 0.2–2.0%. Depending on the intake amount and individual sensitivity, it causes skin symptoms, allergic rhinitis, asthma, and anaphylaxis, which pose a significant health risk to sensitive consumers (Savage et al., 2007). Currently, there is no straightforward cure for food allergy, and avoiding sensitive foods is considered the only way to prevent such allergies (Hosu et al., 2018). In addition, excessive food restriction due to the misdiagnosis of food allergy may cause malnutrition and reduce the quality of life of patients (D'Auria et al., 2019). Therefore, the development of a highly sensitive and selective method for detecting food allergies is important for the correct diagnosis and prevention of food allergies.

To address the problems regarding food allergy, food manufacturers and governments place caution marks on processed food along with food allergy-related information (Yeung & Robert, 2018). In addition, the European Union has also established labeling regulations for 14 allergenic food ingredients (Allen et al., 2014). However, they do not include guidelines for the possibility of occurrence of other unreported allergens, and hence the fundamental problem cannot be solved. Therefore, to fundamentally solve this food allergy problem, the allergy detection device needs to be miniaturized such that they can be used conveniently and directly by sensitive consumers, unlike the conventional laboratory methods that involve long operation time.

Enzyme-linked immunosorbent assay (ELISA) (Chen et al., 2021), polymerase chain reaction (PCR) (Villa et al., 2020), high-performance liquid chromatography-mass spectrometry (HPLC-MS/MS) (De Angelis et al., 2017), and liquid chromatography-mass spectrometry (LC-MS) (Korte et al., 2019) are the most commonly used techniques for

* Corresponding author.
E-mail address: jppark@cau.ac.kr (J.P. Park).

https://doi.org/10.1016/j.foodchem.2022.132061
Received 3 September 2021; Received in revised form 3 January 2022; Accepted 3 January 2022
Available online 5 January 2022

detection of food allergens. However, these methods have significant limitations, including cross reactivity (Platteau et al., 2011), lack of multiplexing capability (ELISA) (Cho et al., 2015), time-consuming DNA-based detection (PCR) (Holzhauser & Roder, 2015), relatively long detection time, requirement of expensive equipment (Yang et al., 2018), and limitations associated with the intrinsic specificity of stable isotope-labeled (SIL) peptides (Korte et al., 2019).

There are well-characterized bioreceptors that can act as recognition elements for biosensor development. From among the various bioreceptors such as antibodies (Benede et al., 2018), peptides (Heo et al., 2019;Wu et al., 2018), aptamers (Kim et al., 2020;Wang et al., 2020), and cells (Jiang et al., 2019), we used the M13 phage as a bioreceptor. Phage display is a selection method (called biopanning) for rapid isolation of high affinity peptides for individual targets, such as organic or inorganic materials (Scott and Smith, 1990). Repeating several rounds of biopanning (target immobilization–phage binding–washing–elution–sequencing), peptide-displaying whole phages or linear or cyclic peptides away from phage particles for specific targets can be easily isolated and applied to various biosensor applications (Chung et al., 2014; Nakama et al., 2021). The M13 phage was chosen because it can be used as a scaffold and is associated with the advantages of easy production, purification, and high yield as it can replicate naturally and efficiently in its bacterial host (Branston et al., 2013). Further, from the safety perspective, using the M13 phage as a bioreceptor to develop a biosensor will be effective because it has been previously reported that the M13 phage harmless to the human body (Paczesny & Bielec, 2020). In addition, the M13 phage is more resistant to the environment than well-known bioreceptors such as antibodies (Benede et al., 2018), peptides (Heo et al., 2019; Wu et al., 2018), aptamers (Kim et al., 2020; Wang et al., 2020), and cells (Jiang et al., 2019).

In this study, we aimed to develop a M13 phage-based electrochemical sensor using surface chemistry, which is one of the most recently developed analytical methods, and extend the applicability of our strategy for the specific and sensitive detection of ovomucoid, as shown in Scheme 1 (see Supplementary material). To the best of our knowledge, this is the first time that a whole M13 phage-based electrochemical biosensor capable of specific detection of ovomucoid has been fabricated.

2. Materials and methods

2.1. Chemicals

Ovomucoid purified from chicken egg white and bovine serum albumin (BSA) were obtained from Sigma-Aldrich (St. Louis, MO, USA). 11-Mercaptoundecanoic acid (11-MUA), 1-ethyl-3-(3-dimethylaminopropyl) carbodiimide hydrochloride) (EDC), N-hydroxy succinimide (NHS), and Sulfo-LC-SPDP, used for functionalization of the gold surface, were purchased from Sigma-Aldrich. Phosphate-buffered saline, pH 7.2 (PBS) and 100% EtOH were purchased from Sigma-Aldrich. The bicinchoninic acid (BCA) assay kit was purchased from Pierce Biotechnology (Rockford, IL, USA). 2,2′-Azino-bis(3-ethylbenzothiazoline-6-sulfonic acid) di-ammonium salt (ABTS) was obtained from Sigma-Aldrich (St. Louis, MO, USA). Horseradish peroxidase (HRP)-conjugated anti-M13 monoclonal antibody was purchased from Sino Biological. Unless otherwise stated, all reagents or solutions used were of analytical grade.

2.2. Strain and M13 phage

The *Escherichia coli* strain ER2738, which was obtained from New England Biolabs, was used as a host for infection of the M13 phage. Phage libraries were purchased from New England Biolabs (Ph.D.-C7C and Ph.D.-12mer).

2.3. Biotinylation of ovomucoid

Ovomucoid was conjugated with biotin using the EZ-Link sulfo-NHS-biotinylation kit (Thermo Scientific, USA). For biotin conjugation, 50 mM biotin was mixed with 100 μg of ovomucoid and incubated overnight on ice. Next, purification was performed using a Zeba desalting column to remove non-reacted biotin or residual reagents, and purified biotinylated protein concentration was measured using the BCA assay. The extent of biotin labeling on ovomucoid was determined using the 4′-hydroxyazobenzene-2-carboxylic acid (HABA)/avidin assay.

2.4. Phage display and DNA sequence analysis

Phage display is a rapid and simple method for identification and isolation of high specific peptides specific to target of interest (called biopanning process) (Scott and Smith, 1990). In a biopanning step, random phage library was incubated with target of interest and desired peptides specific for their corresponding target can easily identified. For biopanning against ovomucoid, we used two different peptide libraries. First, the C7C library in which a peptide could form a cyclic or ring structure through disulfide bonding between one of its cysteine residues and the cysteine on the end of pIII protein of M13 phage, was used to screen for an affinity peptide, like 'CXXXXXXXC' structure. Second, a 12-mer peptide library, of peptides displayed linearly on the pIII protein, was used to screen for unique affinity peptides, with a (X_{12})GGGGS structure. Both libraries allow fast screening for two different types of unique affinity peptides with structural differences (cyclic or linear, length).

Streptavidin-coated plates (streptavidin high binding capacity coated 96-well plates (Thermo Scientific, USA) were used for phage display. After adding 1 μL (1.0×10^{11} PFU/mL) of each M13 library to 100 μL (24.75 μg/mL) of biotinylated ovomucoid, the mixture was stirred at 100 rpm for 1 h at room temperature. When the agitation of the phage-protein complex was completed, the streptavidin-coated plate was washed three times repeatedly using 0.1 M PBS, pH 7.2. Thereafter, the phage-protein complex was added to the streptavidin-coated plates and allowed to react at 110 rpm for 10 min to enable the specific binding between avidin and biotin. Then, 1 μL of biotin (0.1 mM) was added to the plate and incubated for 5 min for blocking, followed by repeated washing 10 times using PBST containing 0.1 M PBS with 0.1 % Tween 20. Finally, phages specifically bound to ovomucoid were eluted in 0.2 M Glycine-HCl (pH 2.2) 1 mg/mL BSA solution, and 15 μL of Tris-HCl (pH 9.0) was added for neutralization. Through successful biopanning, a total of five amplified M13 phages were analyzed by using DNA sequencing. DNA sequencing was performed by Solgent (Daejeon, Korea), and yields were calculated for each round.

2.5. Characterization of selected phage candidates using ELISA

ELISA measurements were performed to compare the relative binding affinities of the five M13 phage candidates as follows. First, the streptavidin-coated plate was pre-washed thrice with 200 μL 0.1 M PBS for 5 min each, following which 100 μL biotinylated ovomucoid (24.75 μg/mL) was added to the streptavidin-coated plate and stirred at room temperature for 1 h. Subsequently, the protein solution was removed and 200 μL blocking solution (5% BSA in $NaHCO_3$, pH 8.6) was added and incubated at 4 ℃ for 1.5 h. Then, after repeated washing with 0.5% PBST six times, each phage was added at a concentration of 10^{12} PFU/mL, followed by stirring at 100 rpm at room temperature for 1 h. After washing six times with 0.5 % PBST, horseradish peroxidase (HRP)-conjugated anti-M13 monoclonal antibody (1:2,500 v/v) diluted in -blocking solution was added and the microplate was then incubated for 1 h at 25 °C. Unbound antibody solution was removed, and the microplate was washed again with TBST. Freshly prepared HRP substrates, tetramethylbenzidine (TMB) were introduced to the microplate and the ELISA signal was measured using a microplate spectrophotometer

(Multiskan FC, Thermo Scientific, Waltham, MA, USA) at 405 nm.

2.6. Preparation of M13 phage-based electrochemical sensor

The bare gold electrodes (1 cm × 2 cm) was prepared in silicon wafer using e-beam lithography. A highly uniform gold layer (~200 nm) was deposited onto the silicon wafer bound by a titanium adhesion layer (~20 nm) using e-beam evaporation in National NanoFab Center (Daejeon, Korea). For chemical attachment of M13 phages on gold electrode, we used two different coupling chemicals. In a MUA chemistry, the gold electrodes were cleaned sequentially with ethanol, distilled water, and piranha solution. Then, the bare gold electrodes were first incubated with MUA at room temperature for 14 h to introduce thiol groups. Then, the gold electrode was further incubated with EDC/NHS (800 mM : 200 mM) at room temperature for 1 h. The carboxyl group (–COOH) of MUA and EDC reacted to form the active O-acylisourea intermediate, which then reacted with NHS to form NHS ester. After that, the gold electrode was further incubated with the M13 phage (1.0×10^{12} PFU/mL) at room temperature for 1 h.

In a SPDP chemistry, the cleaned bare gold electrodes with the same method as described previously were incubated with Sulfo-LC-SPDP at room temperature for 1 h to introduce disulfide bond (–S–S–) (Domínguez-Vera et al., 2007), after polishing the gold electrodes. Then, the gold electrode was further incubated with the M13 phage (1.0×10^{12} PFU/mL) at room temperature for 1 h. The activated ester group of Sulfo-LC-SPDP reacted with the amine group in the N-terminal domain. The degree of immobilization of M13 phage to the activated gold chip was measured by SWV measurements.

2.7. Electrochemical measurements (CV, SWV and EIS)

All electrochemical measurements were performed in 2.5 mM ferro/ferricyanide as an electron mediator in 1 M KNO_3. The measurements were performed using CHI 660E (CH Instruments Inc., USA) with Pt wire and Ag/AgCl electrode as auxiliary and reference electrodes, respectively. CV measurements were conducted in the range of −800 to 800 mV with a step potential (MUA-EDC/NHS and Sulfo-LC-SPDP), amplitude, and frequency of 4 mV, 5 mV, and 10 Hz, respectively. EIS measurements were conducted at the constant voltage value, and at the frequency range of 10^{-2} to 10^{5} Hz (amplitude of 10 mM). In addition, SWV measurements were conducted with two different step potential (-400 to 800 mV in MUA-EDC/NHS chemistry, −800 to −300 mV in Sulfo-LC-SPDP chemistry), amplitude, and frequency of 5 mV and 10 Hz, respectively. The relative current change (ΔI %) in SWV was calculated using the following relationship based on the decreased peak current obtained after immobilization of M13 phages and ovomucoid interaction:

$$\Delta I\ \% = (I_0 – I)/I_0 \times 100$$

where I_o refers to gold-phage oxidation current before addition of protein and I to the gold-protein oxidation current.

2.8. XPS, FT-IR and AFM analysis

Both X-ray photoelectron spectroscopy (XPS) and fourier transform-infrared spectroscopy (FT-IR) were performed to characterize the functionalized gold electrodes which chemically modified and covalently attached whole phages. The XPS experiments were carried out using K-Alpha^{+} (Thermo Scientific, USA). The high-resolution survey spectrum was recorded using Al K-Alpha X-ray source and a pass energy of 200 eV at a step size of 1.0 eV. The FT-IR spectrum was collected using FT/IR-6600 spectrometer (JASCO, Japan) within a range of 3600 to 1200 cm^{-1}, 30 scans at 4 cm^{-1} resolutions. Both spectrums were taken at different gold surface (bare gold surface, MUA treated gold surface, MUA-EDC/NHS treated gold surface and whole phage-tethered gold surface.

Atomic force microscopy (AFM) was performed using an XE-100 atomic force microscope (Park Systems, Suwon, Korea) in National NanoFab Center (Daejeon, Korea) for surface characterization of covalently attached whole M13 phage on the gold electrode. In detail, all topographic images were obtained with a scan rate of 0.8 Hz, 20.8 nm set point, and 33.84 nm amplitude in non-contact mode with cantilevers (Nanoworld AG, Neuchatel, Switzerland). After successful analysis, image processing and analysis were conducted using the XEI offline software provided by Park Systems.

2.9. Computational modeling of affinity peptide-protein interactions

The CABS-dock (http://biocomp.chem.uw.edu.pl/CABSdock) was used to predict specific peptide-protein interactions, giving significant conformational flexibility, interaction similarity and energy optimization to input affinity peptide sequence (CTDKASSSC) and ovomucoid protein ID PDB, IROR. For this analysis, default settings were selected and run 10,000 times on peptide-protein complex, the best model was selected for each affinity peptide complex, and pairs of affinity peptide/ovomucoid residues closer than 4.5 Å.

2.10. Preparation of egg white and white wine for real sample analysis

Egg white and white wine were used as a real sample matrix for the evaluation of our sensor. First, egg whites were separated from yolks and homogenized in an ice bath for 30 min. Then, 10 g homogenized egg whites were adjusted to 50 mL with PBS (100 mM, pH 7.2) and incubated in an ice bath for 6 h. The resulting solution was centrifuged at 15,000 rpm, 4 °C, for 30 min and the supernatant was used for further characterization (Zhu & Sun, 2014; Arabzadeh & Salimi, 2015; Khumsap et al., 2021). White wine was also selected as another food matrix because it possibly contained small amounts of ovomucoid (Khumsap et al., 2021). For preparation experiments, white wine was purchased from local market in Anseong city, Korea and it was pre-treated with dialysis membrane (MWCO: 13 kDa, Wako Pure Chemical Corporation, Tokyo, Japan) to remove the interferences of phenolic compounds according to the previous report (Khumsap et al., 2021). Known amounts of ovomucoid (1.55, 6.19, and 24.75 μg/mL) were spiked in the wine sample and the final products were applied to developed phage sensor without further purification. All the experiments were conducted in six times.

3. Results and discussion

3.1. Identification of ovomucoid-binding phage particles

In total, four rounds of biopanning with two different random peptide libraries (Ph.D.-C7C and Ph.D.-12mer) were performed separately to identify the M13 phage capable of specific binding to ovomucoid. The yield during biopanning with Ph.D.-C7C tended to decrease for a while as it progressed from rounds two to three, although the overall yield increased. However, the yield of biopanning with Ph.D.-12mer library gradually increased as it progressed from the first to the fourth round (Table S1). In both biopanning experiments using different types of peptide libraries, conserved peptide sequences were analyzed using DNA sequencing (Table S2). Through successful sequence analysis, we selected five candidates, and their relative binding affinities for ovomucoid were measured using ELISA (Fig. 1). In biopanning with the Ph.D.-C7C library, C7C 2–12 phages had a higher affinity than C7C 3–26 phages, as shown in Fig. 1A. From these observations, we chose C7C 2–12 phages for further characterization. Next, we tested the binding affinities of C7C 2–12 phages at different phage concentrations. The results showed that binding affinity of C7C 2–12 phages increased with increasing phage concentration within a range of 10^{8}–10^{12} PFU/mL (Fig. 1B). This is not surprising because there are generally three to five

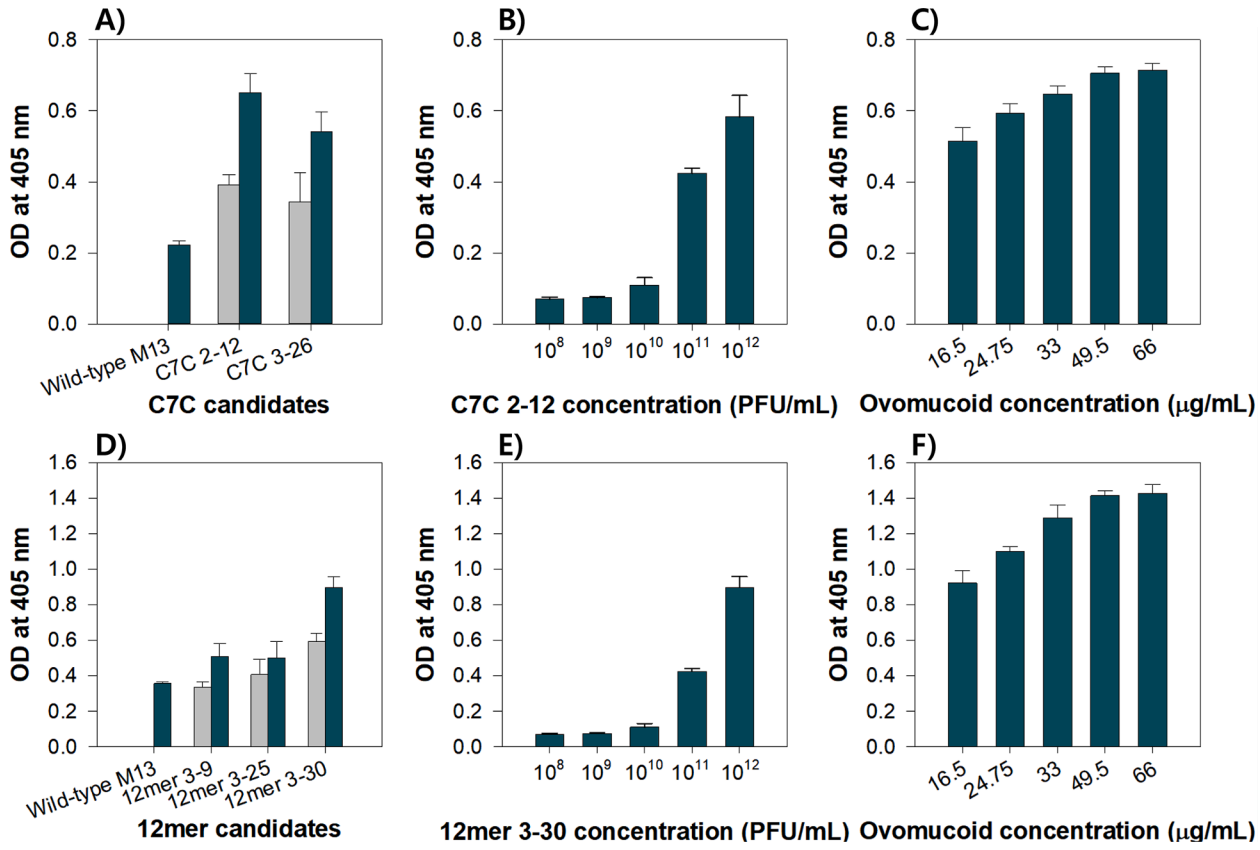

Fig. 1. Characterization of the selected cyclic (C7C) and linear (12mer) whole phages by ELISA (A–C for C7C 2–12, D–F for 12mer 3–30). The gray bar indicates BSA (control) and the green bar indicates ovomucoid. All measurements were performed in triplicate and error bars represent standard deviations. (For interpretation of the references to colour in this figure legend, the reader is referred to the web version of this article.)

copies of peptides per phage. It is likely that binding interaction of the peptides could increase with varying densities and local concentrations. We then tested the binding affinity at different ovomucoid concentrations. It was found that the relative binding affinity of C7C 2–12 phages increased in proportion with the ovomucoid protein concentration (Fig. 1C). In case of biopanning with the Ph.D.-12mer library, the binding affinity of three candidates (12mer 3–9, 12mer 3–25, and 12mer 3–30 phage) was tested using ELISA (Fig. 1D–F). In fact, 12mer 3–30 phages showed the highest binding to ovomucoid. Subsequently, the binding abilities of the selected 12mer 3–30 phage clones at different phage concentrations (10^8 –10^{12} PFU/mL) and ovomucoid concentrations (16.5–66 μg/mL) were measured. As the phage and protein concentration increased, the signal of absorbance also increased (Fig. 2E and F). However, we also found that selected phages still can bind to BSA as control (Fig. 1A and 1D). This is likely that there are rich in hydrophobic (e.g. Met, Ala, Trp, Pro, Leu) and serine residues, indicating that hydrophobic interactions and/or hydrogen bonds are concerned in the binding of BSA. In addition, total contents of surface coat proteins (from pVI to pIX), except pIII on M13 phage might be increased as the increase of phage concentration and this would be possibly interacted with BSA. As shown in Fig. S1, the binding interactions between peptide-displayed phage clones (C7C 2–12 and 12mer 3–30) were almost similar, not quite different at fixed phage concentration (~10^{12} PFU/mL). The results of these experiments indicated that the C7C 2–12 and 12mer 3–30 could use as phage virus-based receptors for highly selective and specific detection of ovomucoid, although little non-specific binding interaction was observed.

3.2. Development of phage virus-based sensor

3.2.1. Selection of chemical linker

Specific and stable immobilization of the receptor on the sensor surface are considered key parameters for biosensor development because these features could affect sensor performance (Xu et al., 2019). First, both different chemical linkers (MUA-EDC/NHS and Sulfo-LC-SPDP) were tested for specific immobilization of whole phages on the gold surface. On the basis of M13 genome, we chose pVIII protein as the anchoring motif for immobilization of the whole phage particle on the gold surface. The pVIII protein was chosen because it has approximately ~ 2700 copies per phage and could be used for chemical attachment of the M13 phage on the gold electrode via covalent attachment through EDC/NHS or Sulfo-LC-SPDP chemistry which is able to react with the amine group in the *N*-terminal domain of the pVIII protein (Chung et al., 2014). In EDC/NHS chemistry, we tried to optimize the best concentration ratio between EDC and NHS for surface chemistry and covalent attachment of the whole phage on the gold electrode. After the alkanethiol self-assembled monolayer with MUA at different concentrations on the gold electrode, the carboxylic group on the end was activated with succinimide esters between EDC and NHS using different concentration ratios and the covalent attachment of phage particles was confirmed by FT-IR and XPS and binding interactions were monitored by SWV measurements. In both FT-IR and XPS measurements, the increase of peak which assigned to the O═C–N bonds at 1650 cm^{-1}) in FT-IR spectrum and the peak of –COO– groups in XPS were clearly observed, while the peak of gold orbital (Au 4d, Au 4p) was decreased in XPS. Note that C7C 2–12 and 12mer 3–30 whole phage particles are covalently attached on the gold electrode via amide bonding, as expected (Fig. S2 and S3). As shown in Fig. 2A and B, the attachment of both whole phage particles (C7C 2–12 and 12mer 3–30) resulted in higher binding at a

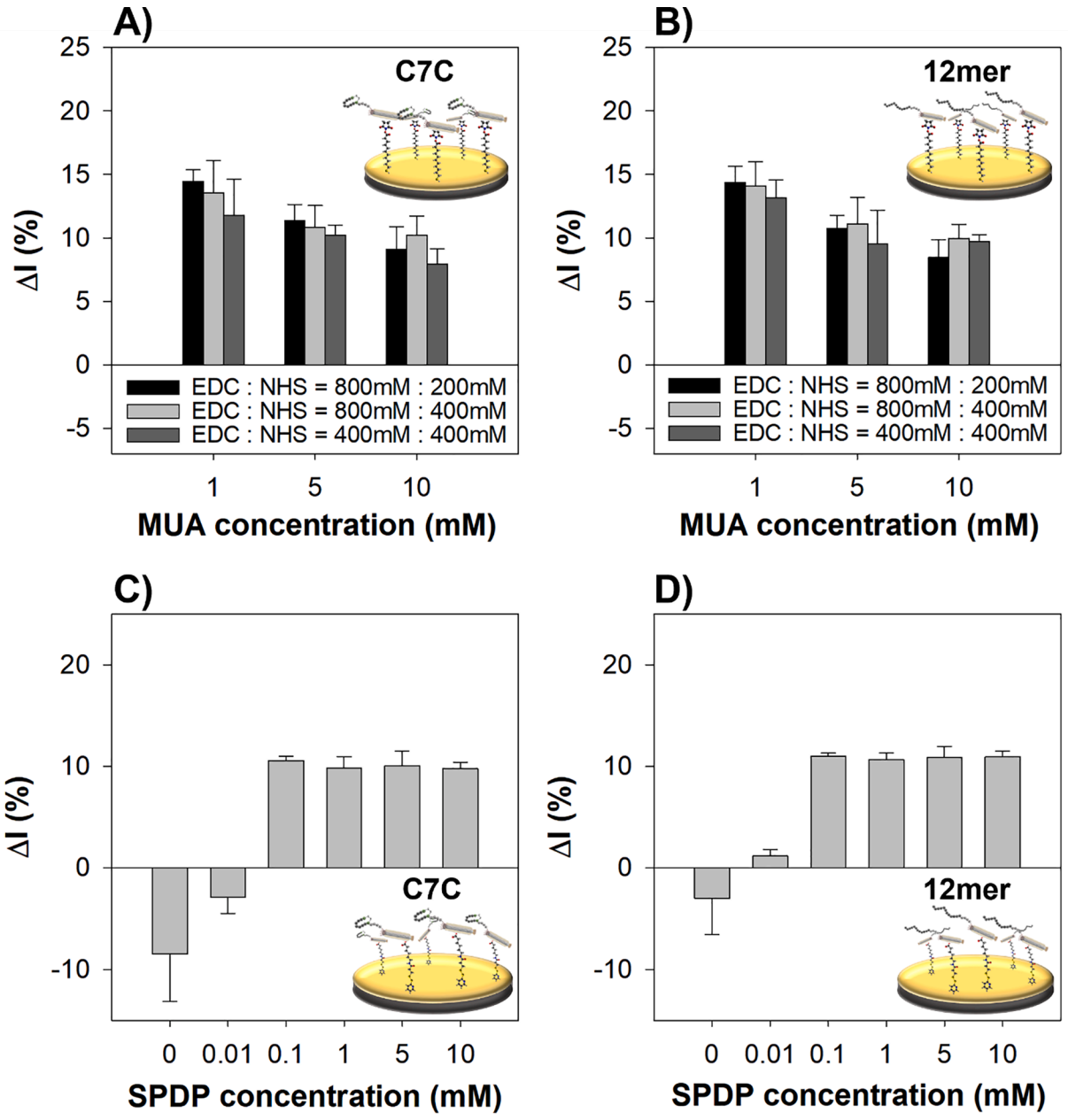

Fig. 2. Optimization of chemically covalent attachment of whole phages on a gold electrode using MUA-EDC/NHS (A and B) and SPDP (C and D). All measurements were performed in triplicate and error bars represent standard deviations.

EDC : NHS (800 mM : 200 mM) ratio on MUA (1 mM)-modified gold electrode, and gradually decreased with increasing MUA concentration in the range of 5–10 mM. The results also showed that C7C 2–12 whole phages had better binding to the modified gold electrode compared to 12mer 3–30 phages. As shown in Table S3, electroactive surface area when C7C 2–12 phages were covalently attached on the gold electrode with MUA chemistry was smaller than those of SPDP chemistry, resulting in much less internal voids and/or roughness on the gold electrode. This could be contributed to mass attachment of C7C 2–12 phages and the amount of electrochemical reaction site for electrochemical ovomucoid detection over the potential sweep.

We also tested the use of SPDP as a coupling linker for covalent chemical immobilization between both whole phages and the modified gold electrode. As expected, the coupling reaction between the activated ester of SPDP and amino groups of pVIII of the whole phages enables covalent attachment of phage particles on the gold electrode. The covalent attachment of both whole phages on the modified gold electrode was accompanied by a decrease in relative current change (ΔI %) with a range of 01–0.01 mM SPDP concentration and comparable within 0.1–10 mM of SPDP, as shown in Fig. 2C, D and Fig. S4.

3.2.2. *Effect of scan rate on electrochemical behavior of modified gold electrodes*

To confirm whether whole M13 phages could be successfully immobilized on the gold surface, the change in current with different scan rates was observed using CV (Fig. S5). As mentioned above, both chemical cross linkers, MUA-EDC/NHS and SPDP were used for the modification of the gold electrode and optimal coupling conditions were also investigated. In an electrochemical sensor, electrical conductivity along with electroactive surface area on the developed sensor interface are considered dominant factors for the detection of targets. Therefore, CV measurements were performed to characterize the electrochemical behavior of whole phage particles on the chemically modified gold electrode. The results revealed that both anodic and cathodic peak

currents with successive attachment of C7C 2–12 whole phages on MUA-EDC/NHS- or SPDP-modified gold electrode increased with increasing scan rate, indicating reversible redox electrochemical reaction on both electrodes (Fig. S5 A-B for MUA-EDC/NHS, Fig. S5 C-D for SPDP, Fig. S6).

For electrodes with immobilized C7C 2–12 phages, a higher value of redox peak was observed with the SPDP-modified gold electrode than the MUA-EDC/NHS-modified gold electrode. This arises probably from the fact that massively bound C7C 2–12 phages could block the gold electrode surface and hinder electron transfer. It is noteworthy that the electrode modified with SPDP is chemically unstable compared to those modified with EDC/NHS. A similar trend was observed for the 12mer 3–30 attached electrode (Fig. S4 E-H). We assumed that this result may be attribute to the electroactive surface area on the modified gold electrode and subsequent electron redox reaction derived from charge transfer kinetics (Matsubara et al., 2016; Kondo et al., 2014). For our hypothesis, we calculated the electroactive surface area (A) of functionalized gold electrodes by CV measurements according to the Randles-Sevcik equation; $i_p = (2.69 \times 10^5)\, n^{3/2}\, A\, D^{1/2} C\, v^{1/2}$. As shown in Table S3, the electroactive surface area of 0.05 cm^2 for bare gold electrode were acquired. However, the electroactive surface area for both functionalized gold electrodes with MUA-EDC/NHS chemistry are much smaller (~0.02 cm^2) than those of gold electrodes with SPDP chemistry (~0.04 cm^2), which suggested strong evidence for massive attachment of whole phage particles on an MUA pre-functionalized electrode, resulting in the increase of resistance and subsequently the decrease of current in CV. From these observations and data analysis, it can be concluded that the attachment and immobilization of a higher number of whole phages on the gold surface can be achieved by using the MUA-EDC/NHS coupling chemistry, whereas the Sulfo-LC-SPDP chemistry cannot provide the same level of immobilization.

3.3. Characterization of chemically modified M13 phage-based electrochemical sensor

3.3.1. Effect of phage concentration and protein concentration

The ability to detect ovomucoid of a chemically modified whole phage sensor with EDC/NHS and SPDP coupling chemistry was validated with different phage and ovomucoid protein concentrations using SWV and EIS measurements (6.19–49.5 μg/mL). Using both C7C 2–12 and 12mer 3–30 with MUA-EDC/NHS chemistry, the results showed that the value of current in SWV decreased and the value of impedance in EIS increased with increasing phage concentration in the range of 10^6–10^{12} PFU/mL (Fig. 3A and B for C7C 2–12, E and F for 12mer 3–30, Fig. S5). This suggested that the number of ovomucoid-specific peptides displayed on the surface of the phage increases their efficiency in binding ovomucoid. A similar trend was observed with changes in ovomucoid protein concentration (Fig. 3C, D, G, H). We found that the current in SWV gradually decreased, while the impedance showed a stepwise increased in EIS, with increase in the amount of ovomucoid.

3.3.2. Determination of binding constants of developed whole phage sensor

To investigate the equilibrium binding constants of both phage sensors (C7C 2–12 and 12mer 3–30 tethered electrochemical sensor), the same amounts of the phages (10^{12} PFU/mL) were immobilized on the gold chip with MUA-EDC/NHS and SPDP chemistry and incubated with ovomucoid (1.55–66 μg/mL) and the relative current change was measured by SWV. When different chemical linkers were used, the dynamic response in both whole phage sensors was observed, with increasing ovomucoid concentration, resulting in saturation around 24.75 μg/mL (Fig. 4A and B). Based on these observations, we calculated the binding constants (K_d) of both phages (C7C 2–12 and 12mer 3–30), which were found to be 2.36 ± 0.44 μg/mL and 2.74 ± 0.52 μg/mL for MUA-EDC/NHS and 4.65 ± 0.32 μg/mL, 6.20 ± 0.67 μg/mL for Sulfo-LC-SPDP, respectively (Fig. S7). The detection limits (LOD) of both whole phage sensors were calculated using the following equations (Kim et al., 2021):

$$\mathrm{LOD} = 3.3\ \delta/sC$$

where δ and s are the standard deviation of the regression line of the y-intercept and slope of the standard curve, respectively.

The C7C 2–12 phage sensor was found to have a limit of detection of 0.12 μg/mL with MUA-EDC/NHS ($y = 0.83x + 11.44$, $R^2 = 0.99$) and 0.57 μg/mL with Sulfo-LC-SPDP modifications ($y = 0.69x + 3.74$, $R^2 = 0.94$), while 12mer 3–30 had an LOD of 0.54 μg/mL with MUA-EDC/NHS ($y = 0.66x + 8.64$, $R^2 = 0.95$) and 0.63 μg/mL with Sulfo-LC-SPDP modifications ($y = 0.53x + 2.03$, $R^2 = 0.93$). We found that both developed phage sensor had a wide dynamic detection range

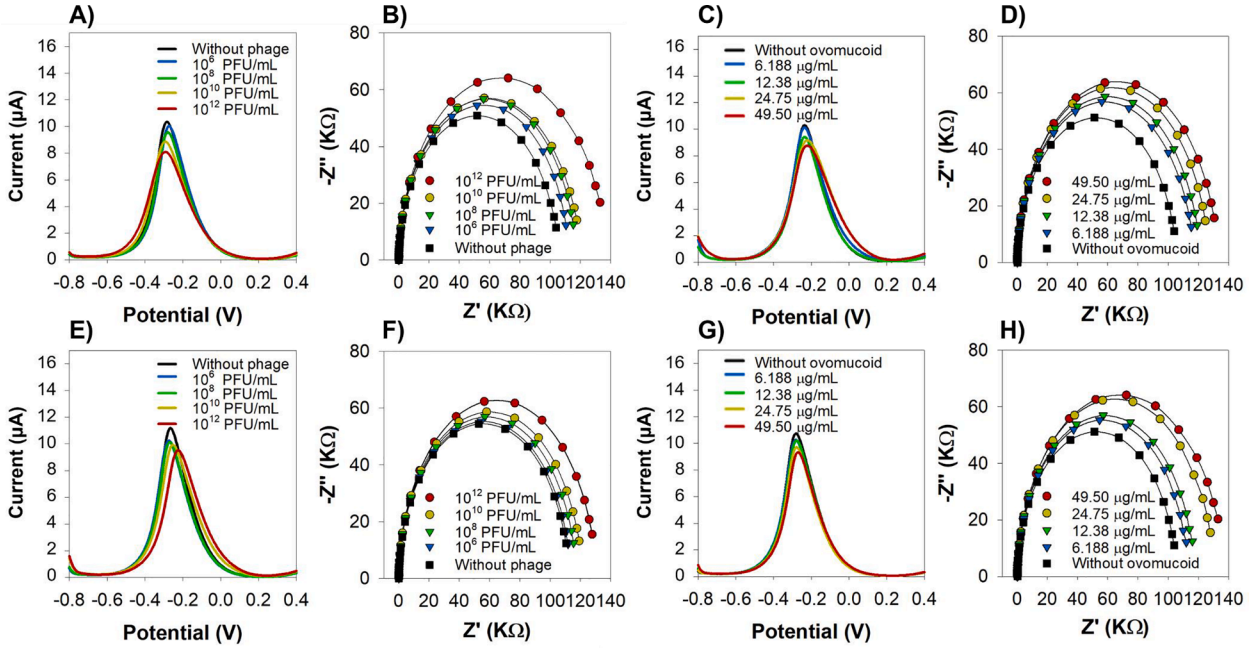

Fig. 3. Characterization of phage sensors (A–D for C7C 2–12, E–H for 12mer 3–30) for the detection of ovomucoid using SWV (A, C, E and G) and EIS (B, D, F and H).

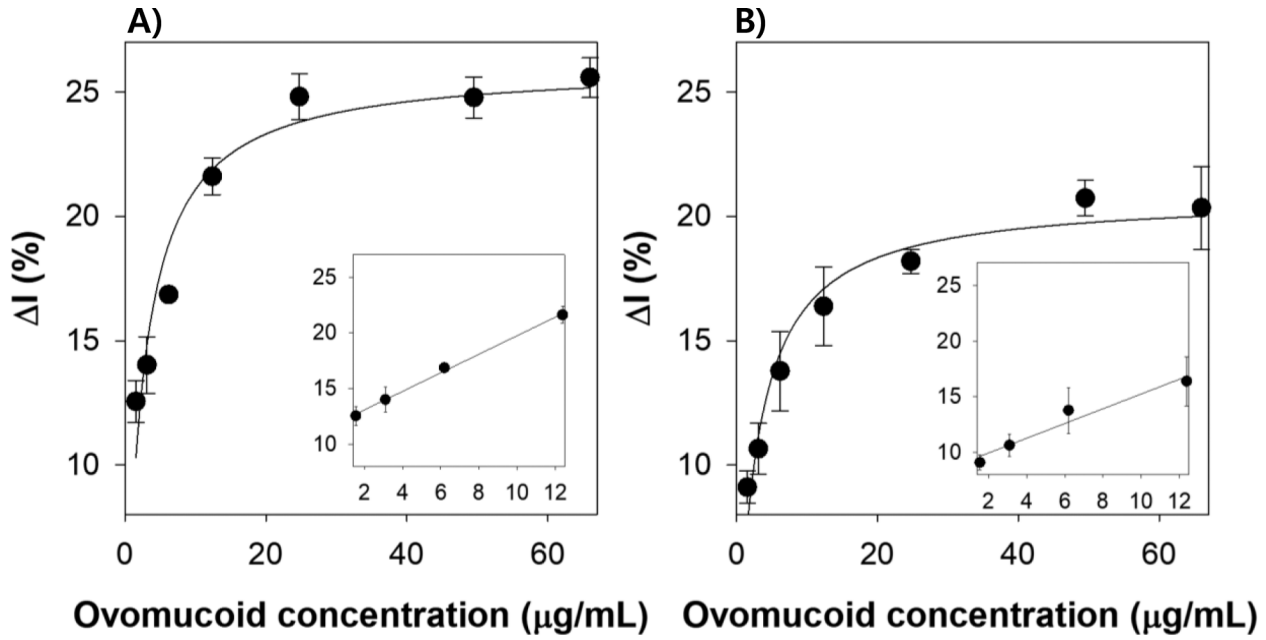

Fig. 4. Determination of equilibrium constant of phage sensor on binding interactions. A) The binding constants (K_d) of phage sensor (C7C 2–12) on the MUA-EDC/NHS-functionalized gold chip. B) The binding constants (K_d) of phage sensor (12mer 3–30) on the MUA-EDC/NHS-functionalized gold chip. All measurements were performed in triplicate and error bars represent standard deviations.

(1.55–12.38 μg/mL), as shown in Fig. 4. Based on these criteria, C7C 2–12 with MUA-EDC/NHS as the coupling linker was the best, resulting in the lowest K_d value and detection limit. We assumed that there are possible reasons of these observations. The structural differences with length of two coupling linker is likely attributed to steric hindrance and orientation of the peptides (cyclic or linear structure) displaying on phage, affecting the accessibility to the ovomucoid.

3.4. Specificity of electrochemical phage sensor

We wanted to test the specificity of the C7C 2–12 phage sensor. For this, the change of ΔI% upon addition of ovomucoid was monitored using SWV measurements with same amounts of phages (10^{12} PFU/mL) and ovomucoid (24.75 μg/mL). As expected, the developed C7C 2–12 phage sensor exhibited specific binding to ovomucoid, while no binding was observed with other proteins tested such as, beta-lactoglobulin,

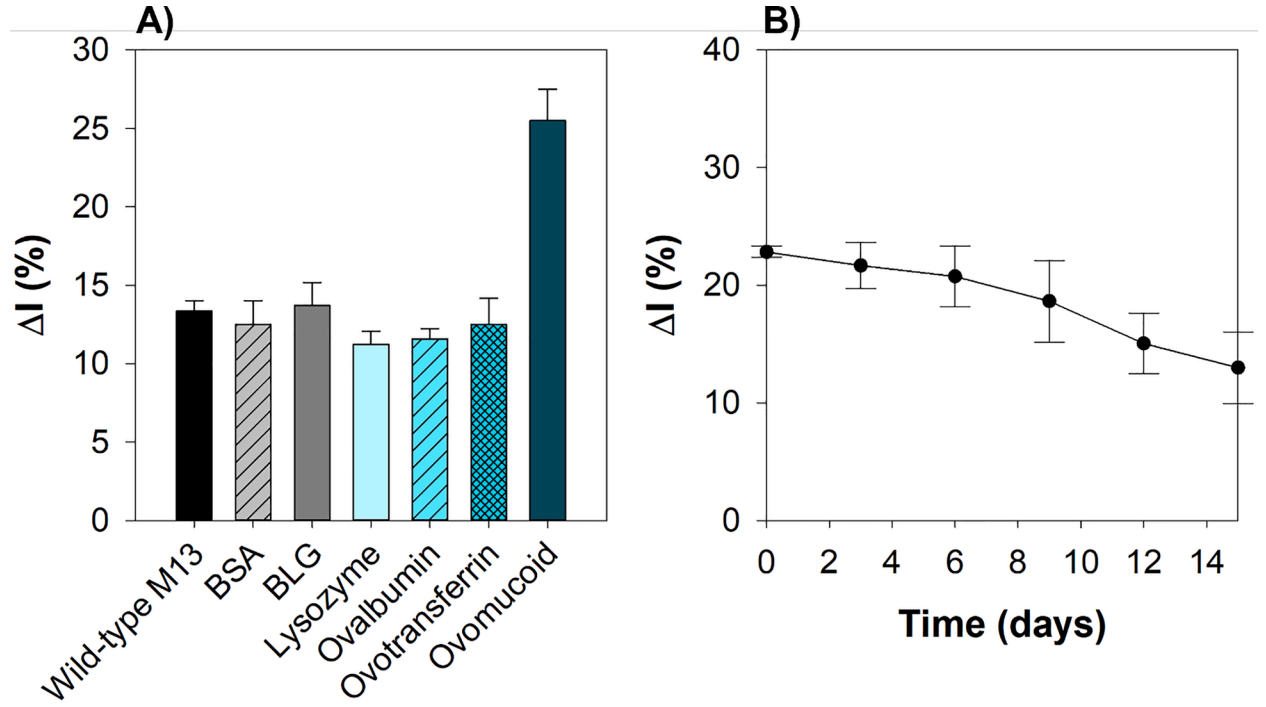

Fig. 5. Specificity and stability of the phage sensor. A) Specificity test of the whole phage sensor (C7C 2–12). B) Stability test of the whole phage sensor (C7C 2–12). The concentrations of all protein solutions were 24.8 μg/mL. Each run was separately performed using a single electrode with successive tests in ovomucoid or other protein solutions, and the change in current (ΔI%) in response to ovomucoid, ovotransferrin, ovalbumin, beta-lactoglobulin (BLG), and BSA was measured by SWV. All measurements were performed in triplicate and error bars represent standard deviations.

ovalbumin, BSA, lysozyme, and ovotransferrin (Fig. 5A). Also, we sequentially tested the performance of 12mer 3–30 phage-tethered sensor under same conditions. From these results, we found that C7C 2–12 phage sensor yielded high specific for ovomucoid, not much of 12mer 3–30 tethered sensor (Fig. S8).

This is probably due to the mass attachment of phage and suitable phage orientation through either side-ways or aligned bundling on the sensor layer (Farooq et al., 2018). In fact, we performed atomic force microscopy (AFM) analysis, suggesting that the monolayer deposition of filamentous M13 phages with fiber-like network (Fig. S9) compared to bare gold electrode as control.

3.5. Reproducibility and stability of electrochemical phage sensor

The reproducibility of the phage-based electrochemical sensor was evaluated by determining the relative current change (ΔI%) with five different electrodes. It was found that the mean ΔI% was 22.89 with a relative standard deviation (RSD) of 4.9%, indicating remarkable reproducibility with good accuracy (Fig. S10). We also tested the operational stability of the phage-based electrochemical sensor for about two weeks (15 days). In order to evaluate stability of the developed sensor, the gold electrodes immobilized with C7C 2–12 phages were stored at 4 °C up to 24 h and then incubated with ovomucoid protein at 25 °C for 1 h, and its current change was measured by SWV. As shown in Fig. 5B, it was relatively stable up to nine days. The results indicated that our developed electrochemical phage sensor had a remarkable stability for further field testing.

3.6. Interference study

We conducted an interference study of the electrochemical phage sensor developed herein in the presence of real sample matrix with solutions where real egg samples and white wine samples were spiked with ovomucoid, respectively. The relative standard deviation (RSD) and percent recoveries were observed in SWV. In our developed phage sensor, the recovery percentages and RSD (%) values were found to be in the range of 97.5–108% and 7.6–9.6% for real egg samples, 97.2–103.8% and 2.2–5.4% for white wine samples. The results showed good recoveries of the phage sensor for detecting ovomucoid in a complex biological sample (Table 1).

3.7. Comparison of analytical performances

There are critical factors for evaluation sensor performance with feasibility in real diagnostics. Among those to be considered, sensitivity and recovery are one of the most important factors. For comparison to other detection methods, the sensitivity of our developed phage sensor system was quite comparable, as it had a good LOD of 0.12 μg/mL, wide dynamic linear range of 1.55–12.38 μg/mL, lower sample volume (~10 μL) and reasonable recovery, as shown in Table S4. Even though ELISA assay can be able to detect ovomucoid with ultra-high sensitivity, polyclonal or monoclonal antibody have been usually used. They are often able to denature or deactivate under high temperature conditions or other harsh environments. In addition, mass production of antibodies is time-consuming step and very expensive. In contrast to antibodies, peptide-displayed phage particle or peptides away from phages have several advantages that can be applied for biosensor developments: i) peptide-displayed phage can be easily produce and cost-effectively purify, ii) peptide-displayed phages can be more amenable for chemical or genetic modification, iii) peptide-displayed phage or peptide away from phages can be effectively incorporated onto the sensor layer for developing electrochemical biosensor. However, it is essential to develop feasible strategies to improve their binding affinities and selectivities over antibodies for various biosensing applications.

Table 1
Analytical results of ovomucoid detection in the presence of real egg white and white wine.

Added concentration (μg/mL)	Found concentration (μg/mL)		RSD (%, n = 6)		Recovery (%)	
	Egg white	White wine	Egg white	White wine	Egg white	White wine
1.55	1.51 ± 0.15	1.55 ± 0.03	9.64	2.20	97.50 ± 9.40	99.80 ± 2.19
6.19	6.45 ± 0.60	6.42 ± 0.25	9.21	3.91	104.0 ± 9.60	103.76 ± 4.06
24.75	26.78 ± 2.04	24.05 ± 1.29	7.60	5.36	108.0 ± 8.23	97.15 ± 5.21

3.8. Molecular docking study between affinity peptide and ovomucoid

It is noteworthy that the specific interaction between affinity peptide and their corresponding target protein plays an important role to understand properly the effectiveness of the biosensor. We used CABS-dock tool to predict binding interactions between peptide and ovomucoid. In the peptide-protein modeling, the fundamental principle is that clustering occurs due to the long-range electrostatic and/or desolvation forces and lead the proteins to a low free-energy attractor at the binding region in ranging from 4 to 9 Å (Kozakov et al., 2005). The results showed that the average RMSD (root mean square deviation) value of computational modeling was found to be 4.66 Å, which is calculated on the peptide only, while average RMSD was closer than 4.5 Å after superimposition of the receptor structures and pairs of peptide/protein residues, suggesting that twenty-three amino acids on ovomucoid protein may involve in the binding to affinity peptide (CTDKASSSC): Ser159, Gly160, Asn158, Lys29, Thr30, Asn158, Thr30, Tyr31, Asn158, Ser156, Ile165, Asn163, Asn158, Gly157, Tyr167, Asn36, Tyr31, Ala40, Glu43, Asn39, Asn36, Ser130. The results indicate that 23 amino acids in ovomucoid are probably the dominant binding sites in the binding to affinity peptides, and the electrostatic interaction and/or desolvation free energy may also involve on the binding interaction, as shown in Fig. S11. Further characterization with synthetic peptides away from phage particles for ovomucoid and comparison with the results from wet experiments will be performed.

4. Conclusions

In summary, a novel approach with a highly sensitive and reliable electrochemical whole phage sensor was demonstrated. In particular, we biopanned two different peptide libraries (C7C and 12-mer) and identified a unique and short affinity peptide that binds to ovomucoid, a known food allergen. The covalent attachment of whole phage particle on the gold sensor layer was optimized with two different coupling chemistries, MUA-EDC/NHS and SPDP as linkers. Under optimal coupling reactions, a phage virus-based electrochemical sensor was developed and characterized for the detection of ovomucoid. The developed C7C 2–12 phage sensor with EDC/NHS chemistry possesses feasible and remarkable sensor performance as well as high sensitivity and binding affinity. Moreover, a good recovery percentage was observed with real egg samples. This approach could be used as not only an alternative to conventional receptors, antibodies, and/or aptamers for on-site practical testing, but also be easily applied to various nanomaterials to improve both the stability and sensitivity of the sensor.

CRediT authorship contribution statement

Jae Hwan Shin: Writing – original draft, Conceptualization, Methodology, Data curation. **Tae Jung Park:** Writing – review & editing. **Moon Seop Hyun:** Methodology, Data curation, Formal analysis. **Jong Pil Park:** Supervision, Conceptualization, Writing – review & editing, Funding acquisition.

Declaration of Competing Interest

The authors declare that they have no known competing financial interests or personal relationships that could have appeared to influence the work reported in this paper.

Acknowledgments

This work was supported by a National Research Foundation of Korea (NRF) grant funded by the Ministry of Science and ICT (2019R1A2C2084065, 2021R1A4A1022206).

Appendix A. Supplementary data

Supplementary data to this article can be found online at https://doi.org/10.1016/j.foodchem.2022.132061.

References

Allen, K. J., Turner, P. J., Pawankar, R., Taylor, S., Sicherer, S., Lack, G., … Sampson, H. A. (2014). Precautionary labelling of foods for allergen content: Are we ready for a global framework? *World Allergy Organization Journal, 7*(1), 1–14. https://doi.org/10.1186/1939-4551-7-10

Arabzadeh, A., & Salimi, A. (2015). Novel voltammetric and impedimetric sensor for femtomolar determination of lysozyme based on metal–chelate affinity immobilized onto gold nanoparticles. *Biosensors and Bioelectronics, 74*, 270–276. https://doi.org/10.1016/j.bios.2015.06.019

Benede, S., Ruiz-Valdepenas Montiel, V., Povedano, E., Villalba, M., Mata, L., Galan-Malo, P., … Pingarron, J. M. (2018). Fast amperometric immunoplatform for ovomucoid traces determination in fresh and baked foods. *Sensors and Actuators B: Chemical, 265*, 421–428. https://doi.org/10.1016/j.snb.2018.03.075

Branston, S. D., Stanley, E. C., Ward, J. M., & Keshavarz-Moore, E. (2013). Determination of the survival of bacteriophage M13 from chemical and physical challenges to assist in its sustainable bioprocessing. *Biotechnology and Bioprocess Engineering, 18*(3), 560–566. https://doi.org/10.1007/s12257-012-0776-9

Caubet, J.-C., & Wang, J. (2011). Current understanding of egg allergy. *Pediatric Clinics of North America, 58*(2), 427–xi. https://doi.org/10.1016/j.pcl.2011.02.014

Chen, J., Lin, H., Li, S., Zhao, J., Ahmed, I., Zhi, L., & Li, Z. (2021). Development of a sandwich enzyme-linked immunosorbent assay (ELISA) for the detection of egg residues in processed food products. *Food Analytical Methods, 14*, 1806–1814. https://doi.org/10.1007/s12161-021-02012-5

Cho, C. Y., Nowatzke, W., Oliver, K., & Garber, E. A. E. (2015). Multiplex detection of food allergens and gluten. *Analytical and Bioanalytical Chemistry, 407*(14), 4195–4206. https://doi.org/10.1007/s00216-015-8645-y

Chung, W.-J., Lee, D.-Y., & Yoo, S. Y. (2014). Chemical modulation of M13 bacteriophage and its functional opportunities for nanomedicine. *International Journal of Nanomedicine, 9*, 5825–5836. https://doi.org/10.2147/IJN.S73883

D'Auria, E., Abrahams, M., Zuccotti, G. V., & Venter, C. (2019). Personalized nutrition approach in food allergy: Is it prime time yet? *Nutrients, 11*(2), 359. https://doi.org/10.3390/nu11020359

De Angelis, E., Pilolli, R., & Monaci, L. (2017). Coupling SPE on-line pre-enrichment with HPLC and MS/MS for the sensitive detection of multiple allergens in wine. *Food Control, 73*, 814–820. https://doi.org/10.1016/j.foodcont.2016.09.031

De Martinis, M., Sirufo, M. M., Suppa, M., & Ginaldi, L. (2020). New perspectives in food allergy. *International Journal of Molecular Sciences, 21*(4), 1474. https://doi.org/10.3390/ijms21041474

Domínguez-Vera, J. M., Welte, L., Gálvez, N., Fernández, B., Gómez-Herrero, J., & Zamora, F. (2007). Covalent deposition of ferritin nanoparticles onto gold surfaces. *Nanotechnology, 19*(2), Article 025302. https://doi.org/10.1088/0957-4484/19/02/025302

Farooq, U., Yang, Q., Ullah, M. W., & Wang, S. (2018). Bacterial biosensing: Recent advances in phage-based bioassays and biosensors. *Biosensors and Bioelectronics, 118*, 204–216. https://doi.org/10.1016/j.bios.2018.07.058

Galan-Malo, P., Ortiz, J.-C., Carrascon, V., Razquin, P., & Mata, L. (2019). A study to reduce the allergen contamination in food-contact surfaces at canteen kitchens. *International Journal of Gastronomy and Food Science, 17*, Article 100165. https://doi.org/10.1016/j.ijgfs.2019.100165

Heo, N. S., Oh, S. Y., Ryu, M. Y., Baek, S. H., Park, T. J., Choi, C., … Park, J. P. (2019). Affinity peptide-guided plasmonic biosensor for detection of noroviral protein and human norovirus. *Biotechnology and Bioprocess Engineering, 24*(2), 318–325. https://doi.org/10.1007/s12257-018-0410-6

Holzhauser, T., & Roder, M. (2015). 13 – Polymerase chain reaction (PCR) methods for detecting allergens in foods. *Handbook of Food Allergen Detection and Control, 245–263*. https://doi.org/10.1533/9781782420217.2.245

Hosu, O., Selvolini, G., & Marrazza, G. (2018). Recent advances of immunosensors for detecting food allergens. *Current Opinion in Electrochemistry, 10*, 149–156. https://doi.org/10.1016/j.coelec.2018.05.022

Jiang, D., Ge, P., Wang, L., Jiang, H., Yang, M., Yuan, L., … Ju, X. (2019). A novel electrochemical mast cell-based paper biosensor for the rapid detection of milk allergen casein. *Biosensors and Bioelectronics, 130*, 299–306. https://doi.org/10.1016/j.bios.2019.01.050

Khumsap, T., Bamrungsap, S., Thu, V. T., & Nguyen, L. T. (2021). Epitope-imprinted polydopamine electrochemical sensor for ovalbumin detection. *Bioelectrochemistry, 140*, Article 107805. https://doi.org/10.1016/j.bioelechem.2021.107805

Kim, J. H., Cho, C. H., Shin, J. H., Hyun, M. S., Hwang, E., Park, T. J., & Park, J. P. (2021). Biomimetic isolation of affinity peptides for electrochemical detection of influenza virus antigen. *Sensors and Actuators B: Chemical, 343*, Article 130161. https://doi.org/10.1016/j.snb.2021.130161

Kim, T.-Y., Lim, J. W., Lim, M.-C., Song, N.-E., & Woo, M.-A. (2020). Aptamer-based fluorescent assay for simple and sensitive detection of fipronil in liquid eggs. *Biotechnology and Bioprocess Engineering, 25*(2), 246–254. https://doi.org/10.1007/s12257-019-0358-1

Kondo, T., Tamura, Y., Hoshino, M., Watanabe, T., Aikawa, T., Yuasa, M., & Einaga, Y. (2014). Direct determination of chemical oxygen demand by anodic decomposition of organic compounds at a diamond electrode. *Analytical Chemistry, 86*(16), 8066–8072. https://doi.org/10.1021/ac500919k

Korte, R., Oberleitner, D., & Brockmeyer, J. (2019). Determination of food allergens by LC-MS: Impacts of sample preparation, food matrix, and thermal processing on peptide detectability and quantification. *Journal of Proteomics, 196*, 131–140. https://doi.org/10.1016/j.jprot.2018.11.002

Kozakov, D., Clodfelter, K. H., Vajda, S., & Camacho, C. J. (2005). Optimal clustering for detecting near-native conformations in protein docking. *Biophysical Journal, 89*(2), 867–875. https://doi.org/10.1529/biophysj.104.058768

Matsubara, T., Ujie, M., Yamamoto, T., Akahori, M., Einaga, Y., & Sato, T. (2016). Highly sensitive detection of influenza virus by boron-doped diamond electrode terminated with sialic acid-mimic peptide. *Proceedings of the National Academy of Sciences, 113*(32), 8981–8984. https://doi.org/10.1073/pnas.1603609113

Nakama, K., Sedki, M., & Mulchandani, A. (2021). Label-free chemiresistor biosensor based on reduced graphene oxide and M13 bacteriophage for detection of coliforms. *Analytica Chimica Acta, 1150*, Article 338232. https://doi.org/10.1016/j.aca.2021.338232

Platteau, C., Cucu, T., De Meulenaer, B., Devreese, B., De Loose, M., & Taverniers, I. (2011). Effect of protein glycation in the presence or absence of wheat proteins on detection of soybean proteins by commercial ELISA. *Food Additives & Contaminants: Part A, 28*(2), 127–135. https://doi.org/10.1080/19440049.2010.539627

Savage, J. H., Matsui, E. C., Skripak, J. M., & Wood, R. A. (2007). The natural history of egg allergy. *Journal of Allergy and Clinical Immunology, 120*(6), 1413–1417. https://doi.org/10.1016/j.jaci.2007.09.040

Scott, J. K., & Smith, G. P. (1990). Searching for peptide ligands with an epitope library. *Science, 249*(4967), 386–390. https://doi.org/10.1126/science.1696028

Villa, C., Costa, J., Oliveira, M. B. P. P., & Mafra, I. (2020). Cow's milk allergens: Screening gene markers for the detection of milk ingredients in complex meat products. *Food Control, 108*, Article 106823. https://doi.org/10.1016/j.foodcont.2019.106823

Wang, Y., Li, H., Zhou, J., Qi, Q., & Fu, L. (2020). A colorimetric and fluorescent gold nanoparticle-based dual-mode aptasensor for parvalbumin detection. *Microchemical Journal, 159*, Article 105413. https://doi.org/10.1016/j.microc.2020.105413

Wu, F.-F., Zhou, Y., Zhang, H., Yuan, R., & Chai, Y.-Q. (2018). Electrochemiluminescence peptide-based biosensor with hetero-nanostructures as coreaction accelerator for the ultrasensitive determination of tryptase. *Analytical Chemistry, 90*(3), 2263–2270. https://doi.org/10.1021/acs.analchem.7b04631

Xu, J., Chau, Y., & Lee, Y.-K. (2019). Phage-based electrochemical sensors: a review. *Micromachines, 10*(12), 855. https://doi.org/10.3390/mi10120855

Yang, J. M., Kim, K. R., & Kim, C. S. (2018). Biosensor for rapid and sensitive detection of influenza virus. *Biotechnology and Bioprocess Engineering, 23*(4), 371–382. https://doi.org/10.1007/s12257-018-0220-x

Yeung, J., & Robert, M.-C. (2018). Challenges and path forward on mandatory allergen labeling and voluntary precautionary allergen labeling for a global company. *Journal of AOAC International, 101*(1), 70–76. https://doi.org/10.5740/jaoacint.17-0391

Zhu, J., & Sun, G. (2014). Facile fabrication of hydrophilic nanofibrous membranes with an immobilized metal–chelate affinity complex for selective protein separation. *ACS Applied Materials & Interfaces, 6*(2), 925–932. https://doi.org/10.1021/am4042965